BUTTERWORTH HEINEMANN

Numerical simulation of double diffusive convection in a V-shaped sump

Z. F. Dong and M. A. Ebadian
Department of Mechanical Engineering, Florida International University, Miami, FL, USA

The numerical simulation of double diffusive convection in a V-shaped sump is investigated in this paper. The linear variations of temperature and concentration on the wall of the V-shaped sump are considered to simulate approximately the boundary condition of the liquid region during continuous casting. Solutions are obtained by solving the conservation equations of mass, momentum, energy, and concentration in the boundary-fitted coordinate system. A nonuniform grid is used in the computations. Pure thermal convection and pure solutal convection for the same boundary conditions as double diffusive convection have been analyzed first to explore the flow phenomena by thermal buoyancy force or solutal buoyancy force alone. The double diffusive convection at different buoyancy forces ratios is then investigated. The flow pattern that appeared in the cross section is discussed in detail. It was found that the double diffusive convection flow in the V-shaped sump is dominated by solutal convection, which is characterized by a multilayered flow structure when the buoyancy forces ratio is greater than 10. However, the thermal convection flow prevails on the flow when the buoyancy forces ratio is less than 1. Furthermore, the double diffusive flow in the V-shaped sump becomes weaker as the angle of the V-shape sump decreases. In addition, the effects of Lewis number on the flow pattern are discussed.

Keywords: double diffusive; bouyancy force; V-shaped sump; numerical simulation

Introduction

Continuous casting is a major process in the steel and nonferrous producing industry. It converts the molten steel directly into slabs, blooms, or billets and also provides a high quality of steel with little defect. During the continuous casting of binary alloys, the molten steel is continuously injected into the mold. As the cooling continues, the liquid region appears like V-shaped sump surrounded by the solid region (Figure 1). It is believed that double diffusive convection is an important factor to affect the segregation in the product, which is induced in the liquid region by buoyancy forces caused by the existence of temperature and concentration gradients. Therefore, more and more attention has been concentrated on understanding double diffusive convection in the liquid region. However, a comprehensive model, which includes the double diffusive flow and heat transfer in the solidification process of a binary solution during continuous casting, still remains to be discerned. Alternatively, the whole process could be considered separately, to investigate the relationship of various parameters in continuous casting. Because the liquid region in the continuous casting appears like a V-shaped sump, double diffusive convection in such a sump is investigated in the present research. In addition, inspection of the literature reveals that most of the research emphasizes double diffusive convection in a rectangular enclosure or square cavity rather than the V-shaped sump. Lee's group (1990, 1991a, 1991b) has conducted research on double diffusive convection in a rectangular enclosure with an aspect ratio equal to two. The transient process of natural convection attributable to thermal and solutal gradients has been investigated experimentally or numerically by Lee et al. (1988), Hyun and Lee (1990), and Lee and Hyun (1990). They included assisting flow as well as opposing flow in their investigations. A layered flow structure has been confirmed under appropriate conditions in the case of lateral heating. Han and Kuehn (1991a, 1991b) have studied experimentally and numerically double diffusive natural convection in a vertical rectangular enclosure with an aspect ratio reaching up to four. The layered multicell flow structure in the enclosure for both assisting and opposing flow has been visualized by the Schlieren method and simulated by the numerical method. Beghein et al. (1992) investigated the double diffusive phenomena in a square cavity. Based on the authors' knowledge, the investigation on double diffusive convection in irregular geometry, such as in the V-shaped sump, has not yet been reported. Therefore, the intention of present research is to investigate numerically the double diffusive convection in a V-shaped sump. The thermal boundary conditions subjected to the V-shaped sump are the approximation conditions on the liquid–mush interface in the actual process of solidification of binary solutions. On the other hand, the boundary-fitted coordinate system is applied because of the irregularity of the V-shaped geometry.

Mathematical formulation

Consider the V-shaped sump shown in Figure 2. The Cartesian coordinates are also given in Figure 2. The height of the sump is h and the angle of the V is ψ. Usually, the angle of the V shape

Address reprint requests to Prof. M. A. Ebadian, Department of Mechanical Engineering, Florida International University, University Park, Miami, FL 33199, USA.

Received 31 August 1994; accepted 8 May 1995

Int. J. Heat and Fluid Flow 16: 236–243, 1995

655 Avenue of the Americas, New York, NY 10010

0142-727X/95/$10.00
SSDI 0142-727X(95)00028-O

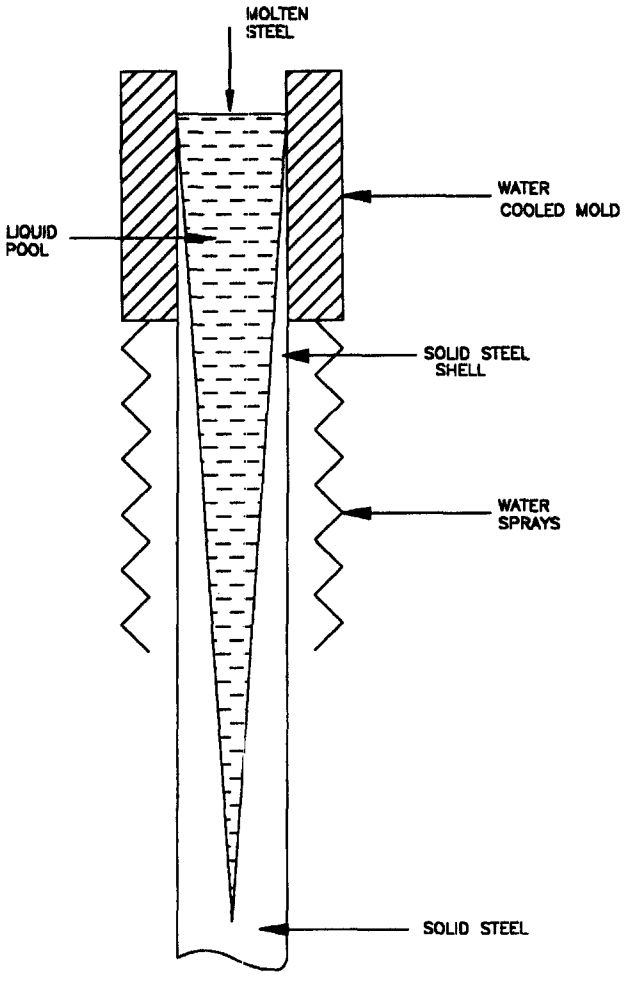

Figure 1 Schematic representation of the continous casting process

formed in the continuous casting is less than 30°. The angle variation is considered in the numerical simulation. The flow in the sump is considered to be two-dimensional (2-D) steady laminar flow. The melton is assumed to be incompressible and Newtonian fluid with negligible viscous dissipation. The thermal properties of the fluid are treated as constants, except for the density in the buoyancy force term, which is approximated by Boussinesq assumption. By employing the above assumptions, the conservation equations of mass, momentum, energy, and heavier species are obtained as follows:

$$\frac{\partial U}{\partial X}+\frac{\partial V}{\partial Y}=0 \tag{1}$$

$$U\frac{\partial U}{\partial X}+V\frac{\partial U}{\partial Y}=-\frac{\partial P}{\partial X}+\mathrm{Pr}\left(\frac{\partial^2 U}{\partial X^2}+\frac{\partial^2 U}{\partial Y^2}\right) \tag{2}$$

$$U\frac{\partial V}{\partial X}+V\frac{\partial V}{\partial Y}=-\frac{\partial P}{\partial Y}+\mathrm{Pr}\left(\frac{\partial^2 V}{\partial X^2}+\frac{\partial^2 V}{\partial Y}\right)+\mathrm{Pr}\,\mathrm{Ra}_t(\theta-SN) \tag{3}$$

$$U\frac{\partial \theta}{\partial X}+V\frac{\partial \theta}{\partial Y}=\frac{\partial \theta}{\partial X^2}+\frac{\partial^2 \theta}{\partial Y^2} \tag{4}$$

$$U\frac{\partial S}{\partial X}+V\frac{\partial S}{\partial Y}=\frac{1}{Le}\left(\frac{\partial^2 S}{\partial X^2}+\frac{\partial^2 S}{\partial Y^2}\right) \tag{5}$$

The equations above have been dimensionalized by using the following parameters:

$$\begin{aligned}
&U=[u/(\alpha_T/h)],\quad V=[v/(\alpha_T/h)],\quad X=x/h,\\
&Y=y/h,\quad P=p/(\rho\alpha_T^2/h^2),\quad \Delta T=T_h-T_\ell,\\
&\Delta c=c_h-c_\ell,\quad \theta=(T-T_\ell)/\Delta T,\\
&S=(c-c_\ell)/\Delta c,\quad \mathrm{Pr}=\nu/\alpha_T,\quad \mathrm{Le}=\alpha_T/D,\\
&\mathrm{Ra}_t=g\beta_t\Delta T h^3/\alpha_T\nu,\quad \mathrm{Ra}_s=g\beta_s\Delta c h^3/\alpha_T\nu,\\
&N=(\beta_s\Delta c)/(\beta_t\Delta T)=\mathrm{Ra}_s/\mathrm{Ra}_t
\end{aligned} \tag{6}$$

In the above dimensionless quantities, the velocities in the x and y

Notation

c	dimensional concentration
D	solutal diffusivity, $M^2\ s^{-1}$
g	gravity, $m\ s^{-2}$
h	height of the cavity, m
j	coefficient, Equation 14
Le	Lewis number, α_T/D
N	buoyancy ratio, $\beta_s\Delta c/\beta_t\Delta T$
Nu	local Nusselt number
$\overline{\mathrm{Nu}}$	mean Nusselt number
P	dimensionless pressure
Pr	Prandtl number, ν/α_T
p	dimensional pressure
Ra	Rayleigh number
Ra_s	solutal Rayleigh number, $g\beta_s\Delta c\ h^3/\alpha_T\nu$
Ra_t	thermal Rayleigh number, $g\beta_t\Delta T\ h^3/\alpha_T\nu$
R_ϕ	general source term, Equation 12
S	dimensionless concentration
T	dimensional temperature, K
U, V	dimensionless velocities
$\bar{U}, \bar{V}$	defined in Equation 13
u, v	dimensional velocities, $m\ s^{-1}$
X, Y	dimensionless coordinates
x, y	dimensional coordinates

Greek

α	coefficient, Equation 14
α_T	thermal diffusivity, $m^2\ s^{-1}$
β	coefficient, Equation 14
β_s	coefficient of volumetric expansion with concentration
β_t	coefficient of volumetric expansion with temperature
Γ_ϕ	general diffusivity, Equation 12
γ	coefficient, Equation 14
Δc	concentration gradient, $c_h - c_\ell$
ΔT	temperature gradient, $T_h - T_\ell$
θ	dimensionless temperature
ν	kinematic viscosity, $m^2\ s^{-1}$
ρ	density, $kg\ m^{-3}$
ϕ	general variables
ψ	angle, Figure 2
ξ, η	coordinates in the computational domain

Subscripts

h	higher value
ℓ	lower value
max	maximum value
min	minimum value

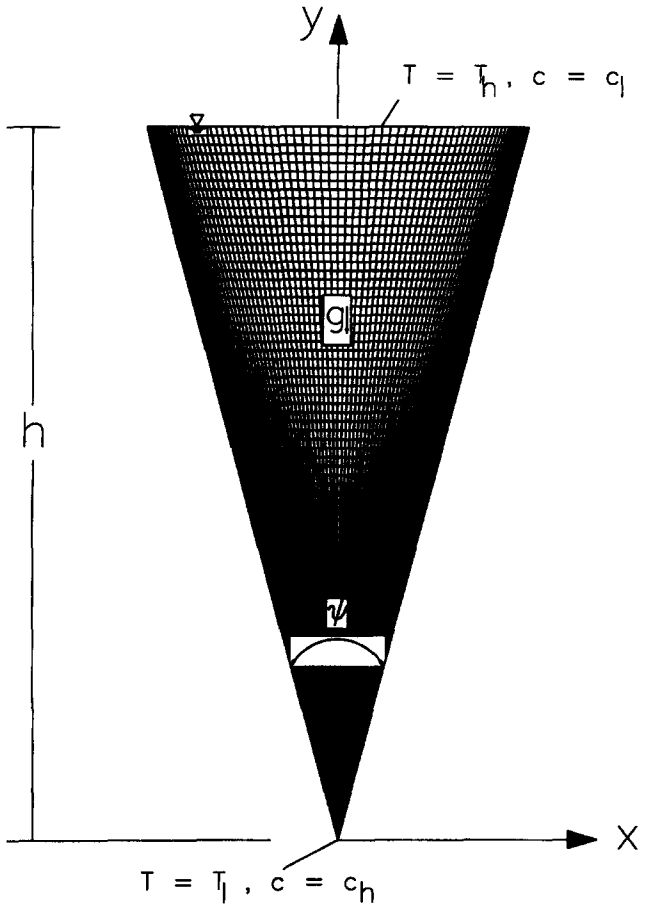

Figure 2 Schematic representation of the V-shaped sump and the grid configuration

directions are denoted as u and v; c, T, and P are concentration (heavy component), temperature, and pressure, respectively. The relevant fluid properties are kinematic viscosity ν; thermal diffusivity α_T; and solutal diffusivity D; and the coefficients of volumetric expansion with temperature and solute are β_t and β_s, respectively. The Prandtl number Pr, the Lewis number Le, the thermal Rayleigh number Ra_t, and the solutal Rayleigh number Ra_s are all included in the governing equations.

It is noted that the moving speed of the solidified solid (or casting speed) with liquid in the core is not considered in the above governing equations, because a quasisteady continuous casting process is assumed. Therefore, a nonslip hydraulic condition has been applied on the inclined walls of the V-shaped sump, which are corresponding to the solid–liquid interfaces. In addition, the normal velocity and shear stress on the free surface are assumed to be zero. These are expressed as follows:

$$U = V = 0 \qquad \text{on the walls;} \tag{7}$$

$$\left.\begin{aligned} V &= 0 \\ \frac{\partial U}{\partial Y} &= 0 \end{aligned}\right\} \qquad \text{on the free surface} \tag{8}$$

An important assumption is made here that the flat free surface of the V-shaped sump is always kept because the liquid melton is continuously injected into the mold during the continuous casting. The thermal boundary conditions applied are higher temperature T_h, which is melton temperature at the top, and lower temperature T_ℓ, which corresponds to solidification temperature at the bottom. The temperature on the walls of the V-shaped sump is assumed to vary linearly. In the present research, we consider the solidification of a hypoeutetic binary solution, thus, the concentration of the solution is higher when the temperature is lower. From this point of view, the concentration of the solution on the solid–liquid interfaces can be approximated by the linear variation from higher concentration c_h at the bottom, to lower concentration c_ℓ at the top. Then, we have the following:

$$\theta = 1; \qquad S = 0 \quad \text{at the top,} \tag{9}$$

$$\theta = 0; \qquad S = 1 \quad \text{at the bottom,} \tag{10}$$

$$\theta = \pm X \operatorname{cotan}(\psi/2) \quad S = 1 \mp X \operatorname{cotan}(\psi 2), \quad \text{on the wall,} \tag{11}$$

where in Equation 11, "+" applies to the right wall and "−" applies to the left wall.

Numerical methodology

The boundary-fitted coordiante system is applied in order to generate the mesh. Consequently, the V-shaped sump in the physical domain is transferred into a rectangle in the computational domain. Accordingly, the governing equations and boundary conditions are also transferred to those in the computational domain and then solved by a control volume-based finite difference method in computational domain. In the present study, the grids are generated by an algebraic method. Nonuniform grid spacing is used in the X-direction with most grids located near the wall, and a uniform grid is adopted in the Y-direction. The resulting grid configuration for $\psi = 30°$ and boundary conditions in the physical domain are shown in Figure 2.

The dimensionless govering equations, Equations 1–5, can be written in a general formation in the boundary-fitted coordinate system:

$$\frac{\partial(\bar{U}\phi)}{\partial\xi} + \frac{\partial(\bar{V}\phi)}{\partial\eta} = \frac{\partial}{\partial\xi}\left[\frac{\Gamma_\phi}{J}\left(\alpha\frac{\partial\phi}{\partial\xi} - \beta\frac{\partial\phi}{\partial\eta}\right)\right] + \frac{\partial}{\partial\eta}\left[\frac{\Gamma_\phi}{J}\left(\gamma\frac{\partial\phi}{\partial\eta} - \beta\frac{\partial\phi}{\partial\xi}\right)\right] + R_\phi \quad , \tag{12}$$

where $\bar{U}$ and $\bar{V}$ are defined as:

$$\bar{U} = U\frac{\partial Y}{\partial\eta} - V\frac{\partial X}{\partial\eta} \quad , \bar{V} = V\frac{\partial X}{\partial\xi} - U\frac{\partial Y}{\partial\xi} \quad , \tag{13}$$

and

$$\begin{aligned} \alpha &= \left(\frac{\partial X}{\partial\eta}\right)^2 + \left(\frac{\partial Y}{\partial\eta}\right)^2 \\ \beta &= \frac{\partial X}{\partial\xi}\frac{\partial X}{\partial\eta} + \frac{\partial Y}{\partial\xi}\frac{\partial Y}{\partial\eta} \\ \gamma &= \left(\frac{\partial X}{\partial\xi}\right)^2 + \left(\frac{\partial Y}{\partial\xi}\right)^2 \\ J &= \frac{\partial X}{\partial\xi}\frac{\partial Y}{\partial\eta} - \frac{\partial X}{\partial\eta}\frac{\partial Y}{\partial\xi} \end{aligned} \tag{14}$$

It is noted that ϕ in Equation 12 is a general variable. When ϕ refers to U, V, θ, or S, the corresponding Γ_ϕ and R_ϕ are the following:

$$\Gamma_u = \mathrm{Pr} \quad , \quad R_u = -\frac{\partial p}{\partial\xi}\frac{\partial Y}{\partial\eta} + \frac{\partial P}{\partial\eta}\frac{\partial Y}{\partial\xi} \tag{15}$$

$$\Gamma_v = \mathrm{Pr} \quad , \quad R_v = J\,\mathrm{Pr}\,\mathrm{Ra}_t(\theta - SN) - \frac{\partial P}{\partial\eta}\frac{\partial X}{\partial\xi} + \frac{\partial P}{\partial\xi}\frac{\partial X}{\partial\eta} \tag{16}$$

$$\Gamma_\theta = 1 \quad , \quad R_\theta = 0 \tag{17}$$

$$\Gamma_s = 1/\mathrm{Le} \quad , \quad R_s = 0 \tag{18}$$

The governing equation, Equation 12, is discreted by a control volume-based finite difference method in the boundary-fitted coordinate system. A staggered grid is employed for the velocity components U and V as well as $\bar{U}$ and $\bar{V}$. A power-law scheme is adopted for the convection–diffusion formulation (Patankar 1980). The coefficients, such as α, β, γ, J, are calculated by second-order central difference approximation. The SIMPLEC algorithm is applied to treat the coupling between pressure and velocities (Van Doormal and Raithby 1984). The solutions are obtained by the ADI method. Also, a block correction scheme is incorporated to accelerate the convergence rate. Underrelaxation is required to secure convergence of the iteration procedure. The range for the underrelaxation factor is $0.2 \sim 0.6$ for velocity, temperature, and concentration. A fully converged solution is reached when the following criterion is satisfied for all nodes:

$$\frac{\| \phi_{ij}^{k+1} - \phi_{ij}^{k} \|_\infty}{\| \phi_{ij}^{k+1} \|_\infty} \leq \varepsilon \quad , \tag{19}$$

where ϕ refers to U, V, θ, and S. Subscript ij represents the node number in the boundary-fitted coordinate system. Superscript k refers to the kth iteration, and $\| \, , \, \|_\infty$ is the infinite norm. ε is a very small number, 10^{-6}. On the other hand, the velocity, temperature, and concentration profile should be symmetric to the symmetry line of the V-shape, while the entire V-shape is taken as the solution domain. This is also a criterion of the convergence. In the computation, the value of ε is adjusted until the solution satisfies all the criteria. The residuals, U, V, θ, and S, are in the order of magnitude of 10^{-5}, when the criterion of convergence is satisfied.

Results and discussion

For the purpose of validating the present numerical code, the natural convection of air in a square enclosure has been numerically analyzed. The results for $\mathrm{Ra} = 10^3 - 10^6$, $\mathrm{Pr} = 0.71$ of the present investigation have been compared with the benchmark results by De Vahl Davis (1983) and Lin et al. (1990). Excellent agreement between them has been achieved. A detailed comparison is provided in Table 1. Nu_{max} and Nu_{min} in Table 1 are the local maximum and minimum Nusselt numbers, respectively. The further comparison for the double diffusive convection in a square enclosure using the present code with those from Beghein et al. (1992) has been made for assisting flow with

Table 1 Comparison of Nusselt numbers for Pr = 0.71

		Nu	Nu_{max}	Nu_{min}
$\mathrm{Ra} = 10^3$	De Vahl Davis (1983)	1.117	1.507	0.692
	Lin et al. (1990)	1.114	1.497	0.717
	Present results	1.119	1.519	0.693
$\mathrm{Ra} = 10^4$	De Vahl Davis (1983)	2.238	3.528	0.586
	Lin et al. (1990)	2.262	3.590	0.587
	Present results	2.248	3.600	0.585
$\mathrm{Ra} = 10^5$	De Vahl Davis (1983)	4.509	7.717	0.729
	Lin et al. (1990)	4.655	8.328	0.743
	Present results	4.567	7.919	0.731
$\mathrm{Ra} = 10^6$	De Vahl Davis (1983)	8.817	17.925	0.989
	Lin et al. (1990)	8.742	19.360	1.009
	Present results	8.774	17.129	1.024

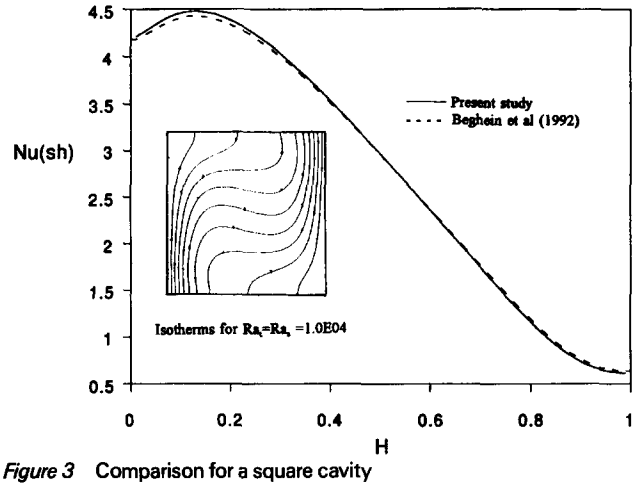

Figure 3 Comparison for a square cavity

parameters of $\mathrm{Le} = 1$, $\mathrm{Pr} = 0.71$, $\mathrm{Ra}_t = \mathrm{Ra}_s = 10^4$. The local Nusselt or Sherwood number distributions along the left vertical wall of the square cavity are compared with those from Beghein et al., shown in Figure 3. The isotherms for that case are also shown in Figure 3, which are identical to the one from Beghein et al. It is found that excellent agreement has been achieved.

Numerical experiments have been conducted to choose the independent grids. The calculation was made for the case of $\psi = 30°$, $\mathrm{N} = 10$, $\mathrm{Le} = 100$, and $\mathrm{Pr} = 7$. Grids of 61×61, 81×81, and 101×101 were used. The flow patterns (streamlines) from the grid of 101×101 and the grid 81×81 are almost identical, and the differences of the values of the velocity on the free surface are less than 2%. However, the computer time consumed for the finer grid is much longer. As an option of compromising between accuracy and computation time, the 81×81 grid applies in all calculations.

In recent years, the aqueous solution has been chosen as the fluid to simulate the solidification of binary alloys (Bennon and Incropera 1988). The fluid with $\mathrm{Pr} = 7$ and $\mathrm{Le} = 100$ is chosen in this analysis, when emphasis is placed on the effects of the buoyancy forces ratio and the angle of the V-shape on the double diffusive convection in the V-shaped sump. For the convenience of comparison, the solutal Rayleigh number is set to 10^6, and ψ is set to 30° to investigate the effects of the buoyancy forces ratio by varying the value of the thermal Rayleigh number. The angle of the V-shape varies from 10 to 30° to determine the effects of the geometry on double diffusive convection at the fixed buoyancy forces ratio, $N = 10$, $\mathrm{Le} = 100$, and $\mathrm{Pr} = 7$, and the Le number effects on the flow are examined afterwards for the V-shape sump with 30°.

First, the pure thermal convection and the pure solutal convection have been calculated in the V-shaped sump with $\psi = 30°$. The flow patterns are shown in Figures 4 and 5 in terms of streamline. The thermal Rayleigh numbers and solutal Rayleigh number are 10^4, 10^5, and 10^6, respectively, and the Prandtl number is equal to seven. Figure 4 displays the flow in the V-shaped sump under the influence of the thermal Rayleigh number alone, and Figure 5 displays the pure solutal convection with different solutal Rayleigh number. It is seen from Figure 4 that the two symmetric vortex flows are located at the top area of the V-shape sump for Rayleigh numbers of 10^4, 10^5, and 10^6. Because the temperature on the wall of the V-shape is linear distributed, and the higher temperature of fluid is at the top, circulation of the vortex is toward the center. Another pair of vortices is close to the walls and relatively weak. On the other hand, the temperature of fluid gradually decreases to the bottom of the V-shaped sump, causing the flow in that area to be much weaker. As Rayleigh numbers

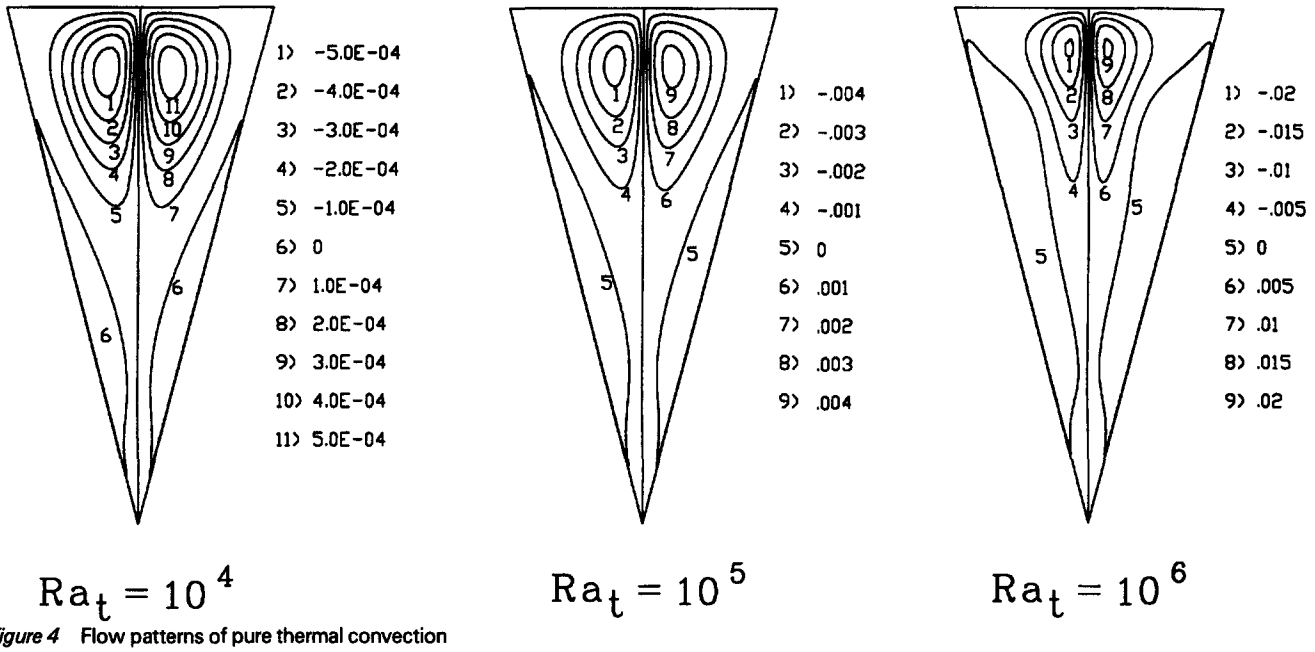

Figure 4 Flow patterns of pure thermal convection

increase, the flow gets stronger. The second pair of vortices near the wall, which is circulated toward walls, takes up more space and pushes the primary vortex to the center. Figure 5 illustrates the solutal convection induced by the buoyancy forces attributable to the concentration gradients in the cases of $Ra_s = 10^4$, 10^5, and 10^6. It is seen that two major pairs of vortices are formed in the cross section of the V-shape sump; the primary vortex formed in the center area and the secondary vortex formed in the area closed to the wall. The direction of flow in the center line is upward to make the circulation of the fluid toward the walls, while the circulation of the second pair of vortex near the boundaries is toward center. As solutal Rayleigh number increases, the secondary vortex becomes stronger and pushes the primary vortex toward the center area. When the solutal Rayleigh number is higher ($Ra_s = 10^6$), the third and fourth pair of vortices appear. However, in this case, the secondary vortex is getting weaker, consequently, the layered flow pattern is established by solutal buoyancy. It follows, by comparison of Figures 4 and 5, that the thermal convection induced by thermal buoyancy force is stronger mostly on the top of the V-shaped sump; whereas, the solutal convection generated by solutal buoyancy force may form a layered flow structure in the case of higher solutal Rayleigh number. In addition, the flow by primary vortex in thermal convection is toward center, which is the opposite direction of the circulation of the vortex induced in the solutal convection.

In Figure 6, the effects of the buoyancy forces ratio on the flow patterns in the double diffusive flow in the V-shaped sump are displayed for $N = 0.1$ to 100. The Pr number and Le number are constants in those cases, equal to 7.0 and 100, respectively. When $N = 0.1$, the solutal Rayleigh number is smaller than the thermal Rayleigh number Ra_t. The flow in the bottom region of the V-shaped sump and near the wall are very weak. This is a typical characteristic of thermal convection. Therefore, the flow is dominated by the thermal convection. However, the major vortex caused by thermal convection is suppressed by the solutal convection, so that the shape of the vortex is changed. The entire

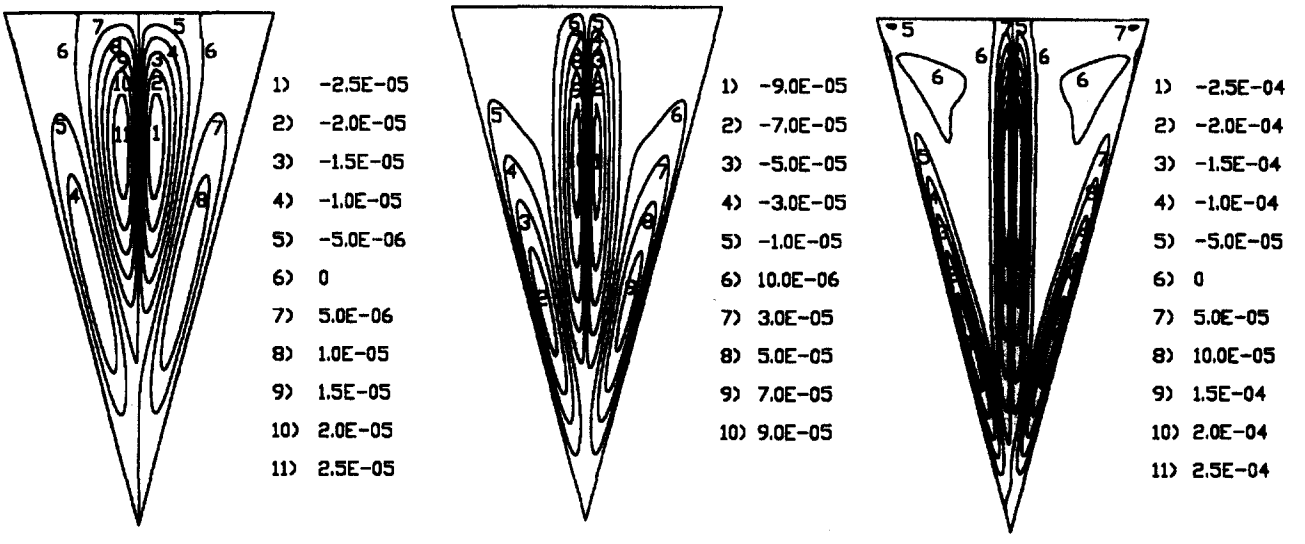

Figure 5 Flow patterns of pure solutal convection

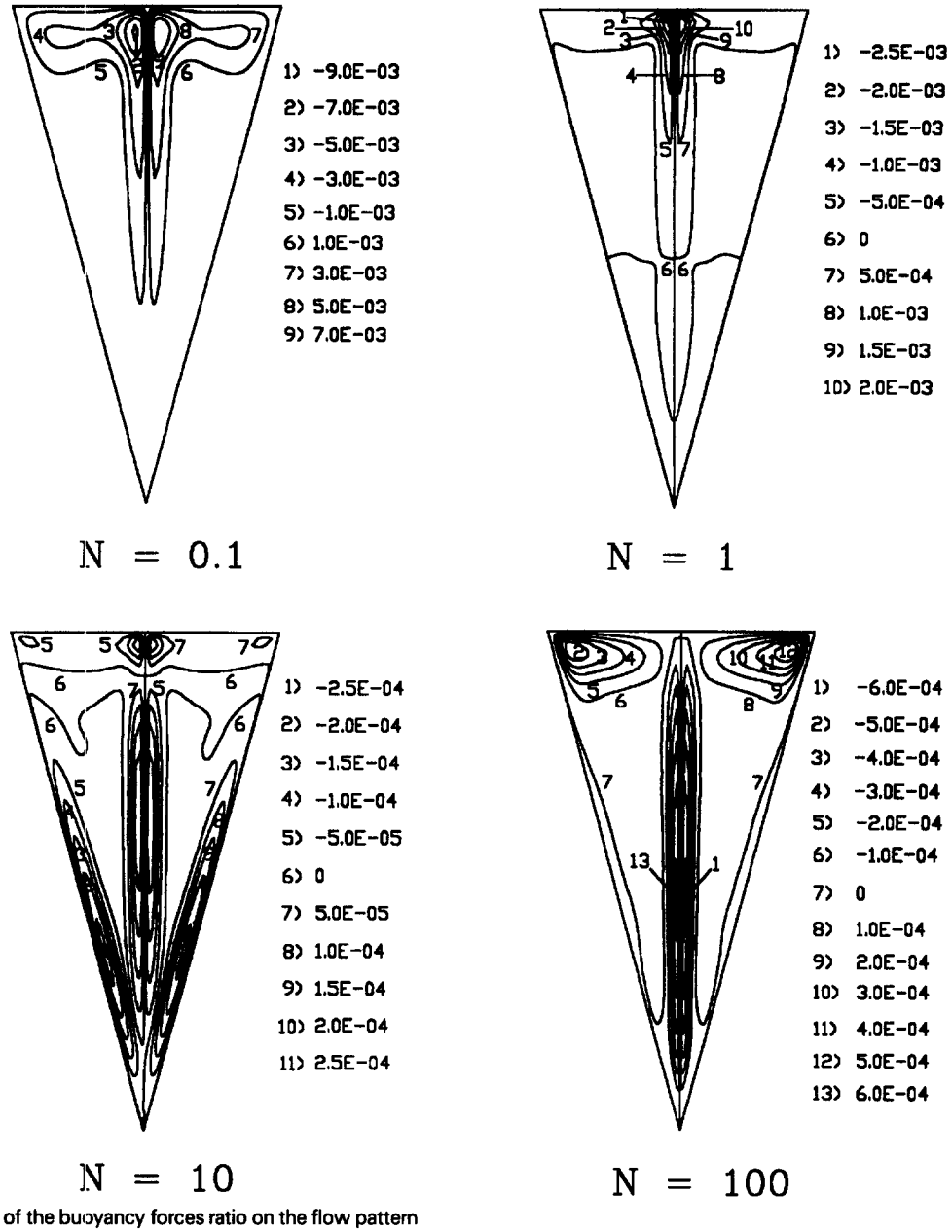

Figure 6 Effects of the buoyancy forces ratio on the flow pattern

pair of vortices takes up the area of the upper part and the center of the V-shaped sump. When $N=1$, the thermal Rayleigh number is equal to the solutal Rayleigh number. Because of the circulations of the vortex generated by thermal convection and the solutal convection are different, the flow in the cross section of the V-shape sump becomes weak. Only a small flow can be seen on the top. As N increases further ($N=10$, $N=100$), the solutal convection dominates the thermal convection. The layered flow structure has been formed. In the case of $N=10$, the several pair of vortices can be found in the cross section of the V-shaped sump. Basically, three layers of flow are detected. When the ratio of the solutal buoyancy force to the thermal buoyancy force increases further ($N=100$), a pair of vortices appears in the corner of the top, and they are relatively stronger, compared to the flow in the center part of the cross section. The three layers of the flow in the case of $N=10$ becomes two layers of flow in the case of $N=100$.

The effects of the angle of V-shaped sump on the flow pattern are displayed in Figure 7. Two angles of 10° and 20° are shown there. The other parameters are Pr = 7.0, Le = 100, N = 10. It is found that the layered flow structure diminishes when the angle of the V-shaped sump decreases. This is because there is less area where the double diffusive convection develops within the cross section of the V-shaped sump. The flow from multilayered flow ($\psi=30°$) is changed into a one layered flow ($\psi=10°$).

Shown in Figure 8 is the effects of the Le number on the flow patterns in V-shaped sump. The Pr number, buoyancy force ratio, and the angle of the V-shaped sump are 7°, 10°, and 30°, respectively. It is seen that the flow in the cross section of the V-shaped sump is obviously dominated by solutal convection with the fluid of higher Le number in the present specific temperature and concentration boundary conditions ($N=10$). The larger value of the Le number means that the fluid has a greater capability of thermal diffusion. Consequently, the flow induced by thermal buoyancy force is weaker than the flow by solutal buoyancy force. Therefore, the flow in the case of Le = 50 is dominated by the solutal convection.

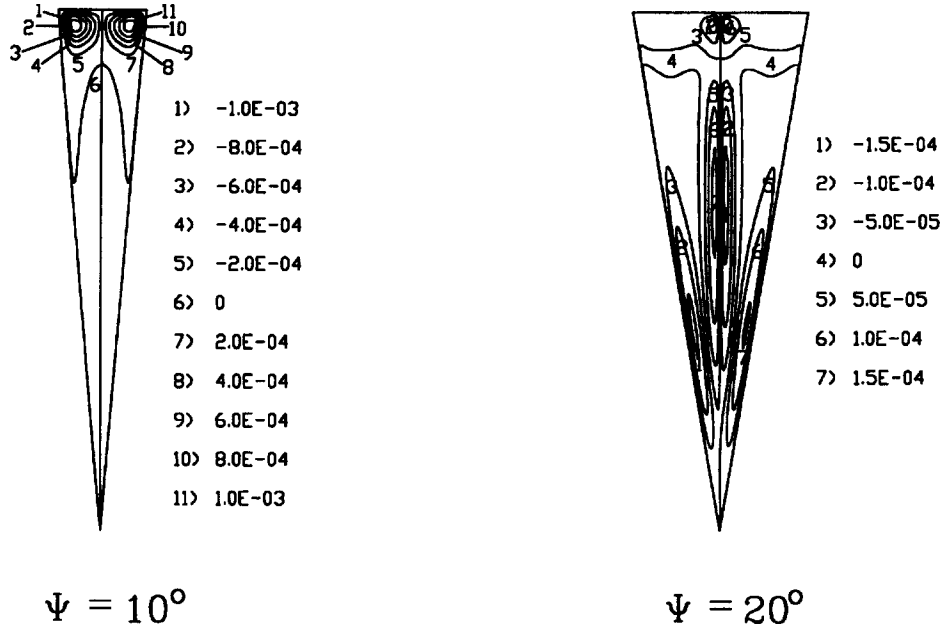

Figure 7 Effects of the angle of V-shaped sump on the flow pattern

In the present analysis, the temperature and concentration distributions are mostly stratified, because the linear distributions of temperature and concentration are subjected to the walls of the V-shaped sump. Therefore, the isothermal and isoconcentration lines for each case are omitted without loss of any important information on flow patterns.

Concluding remarks

The double diffusive convection in a V-shaped sump is numerically simulated in this paper. The boundary-fitted coordinate system is used in the numerial analysis. Pure thermal convection and solutal convection are also calculated. The buoyancy forces ratio effects and the angle of the V-shape on the double diffusive flow are investigated. All analyses are based on the thermal and solutal boundary conditions, which are the approximate simulations of the liquid region of continuous casting. It was found that when the buoyancy forces ratio is greater than 10, the double diffusive flow in the V-shaped sump is dominated by solutal convection and the multilayered flow pattern takes place. When the buoyancy forces ratio is less than one, thermal convection prevails on the flow. Correspondingly, the stronger flow exists on the top of the V-shaped sump. In addition, as the angle of the V-shaped sump decreases, the double diffusive flow becomes weaker and multilayered flow structure diminishes.

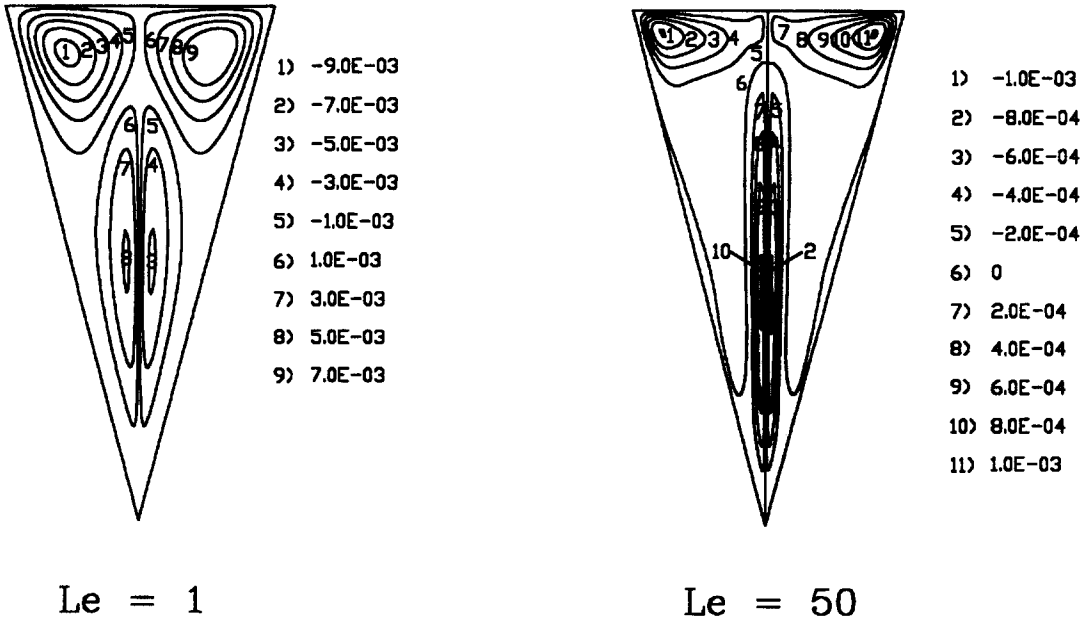

Figure 8 Effects of Lewis number on the flow structure

Acknowledgment

The results presented in this paper were obtained in the course of research sponsored by the National Science Foundation under Grant No. HRD-9250087.

References

Beghein, C., Haghighat, F. and Allard, F. 1992. Numerical study of double diffusive natural convection in a square cavity. *Int. J. Heat Mass Transfer*, **35**, 833–846

Bennon, W. D. and Incropera, F. P. 1988. Numerical simulation of binary solidification in a vertical channel with thermal and solutal mixed convection. *Int. J. Heat Mass Transfer*, **31**, 2147–2160

De Vahl Davis, G. 1983. Natural convection of air in a square cavity, a benchmark numerical solution. *Int. J. Numer. Math. Fluids*, **3**, 249–264

Han, H. and Kuehn, T. H. 1991a. Double diffusive natural convection in a vertical rectangular enclosure—I. Experimental study. *Int. J. Heat Mass Transfer*, **34**, 449–459

Han, H. and Kuehn, T. H. 1991b. Double diffusive natural convection in a vertical rectangular enclosure—II. Numerical study. *Int. J. Heat Mass Transfer*, **34**, 461–471

Hyun, J. M. and Lee, J. W. 1990. Double diffusive convection in a rectangle with cooperating horizontal gradients of temperature and concentration. *Int. J. Heat Mass Transfer*, **33**, 1605–1716

Lee, J. W. and Hyun, J. M. 1990. Double diffusive convection in a rectangle with opposing horizontal temperature and the concentration gradients. *Int. J. Heat Mass Transfer*, **33**, 1619–1622

Lee, J. W. and Hyun, J. M. 1991a. Time-dependent double diffusive convection in a stable stratified fluid under lateral heating. *Int. J. Heat Mass Transfer*, **34**, 2409–2421

Lee, J. W. and Hyun, J. M. 1991b. Double diffusive convection in a cavity under a vertical solutal gradient and a horizontal temperature gradient. *Int. J. Heat Mass Transfer*, **34**, 2403–2427

Lee, J. W., Hyun, J. M. and Kim, K. W. 1988. Natural convection in confined fluids with combined horizontal temperature and concentration gradients. *Int. J. Heat Mass Transfer*, **31**, 1969–1977

Lin, T. F., Huang, C. C. and Chang, T. S. 1990. Transient binary mixture natural convection in square enclosures. *Int. J. Heat Mass Transfer*, **33**, 287–299

Patankar, S. V. 1980. *Numerical Heat Transfer and Fluid Flow*, Hemisphere, Bristol, PA

Van Doormal, J. P. and Raithby, G. D. 1984. Enhancement of the SIMPLE method for predicting incompressible fluid flow. *Num. Heat Transfer*, **7**, 147–163